EURASIAN JOURNAL OF MATHEMATICAL AND COMPUTER APPLICATIONS
ISSN 2306–6172
Volume 2, Issue 2(2014) 5–29

COUPLED PHYSICS ELECTRICAL CONDUCTIVITY IMAGING

A. Tamasan, A. Timonov

Abstract Coupled physics electrical conductivity imaging utilizes interactions between the electric and some other fields, thereby providing useful interior functionals. Combining the interior and boundary data, such couplings are aimed to overcome low resolution inherent to the traditional electrical impedance tomography. In this paper we present a brief overview of some physical and mathematical aspects of coupled physics electrical conductivity imaging.

Key words: coupled physics imaging, p-Laplacian, inverse problems, least gradient problems, algorithms

AMS Mathematics Subject Classification: 35J60, 35J70, 35J92, 35Q60, 35R30, 49M29

1 Introduction

Determining the electrical conductivity was originated in electrical prospecting in [21, 43, 72]. Traditionally, boundary data has been the main information used to image the electrical conductivity of the interior of an object. Methods which seek to recover the electrical conductivity inside the object from measurements of voltages/currents at the boundary have been known as Electrical Impedance Tomography (EIT). Due to the high contrast in the electrical conductivity of biological tissues, a renewed interest in EIT started in the middle of the eighties geared by the applications in medical imaging (see, e.g., [31], which soon exploded in developments on both the mathematics and engineering field. Among some of the most remarkable results on the mathematical facet of EIT we mention [5, 20, 54, 55, 63]. For understanding on the breadth of these development we refer to the review papers [17,18,23]. It is by now well understood that the EIT problem is severely ill-posed and it possesses a logarithmic-type stability [2], which cannot be in general improved (see [50]). The stability of such a type is a manifestation of the low sensitivity of the trace of the voltage potential at the boundary to variations of the electrical conductivity inside the object. As a result, the resolution of EIT is very low.

To increase sensitivity, new methods have been developed that are based on interior measurements. In some cases, such data can be obtained by coupling the primary physical field, which is the electric field, with other fields, such that the interactions between them provide useful interior functionals. Note that in some cases the latter may lead to several different inverse problems In this review we focus on the problem

of recovering the electrical conductivity from the interior data subject to a certain boundary condition.

To date, in the mathematics literature (see, e.g., surveys [10, 59, 73]) there are available a number of papers in which the interior functionals of u or ∇u have been considered. The specific choice of such functionals is determined by the physical nature of the problem, as well as by their sensitivity to variations of the electrical conductivity. To cite several examples, one may indicate a component H_z of the magnetic field $\mathbf{H}$ in Magnetic Resonance EIT, the current density $\mathbf{J}$ or its magnitude $|\mathbf{J}|$ in Current Density Imaging, the power density $\sigma|\nabla u|^2$ in Impedance-Acoustic or Accousto-Electrical, or Thermo-Acoustic Tomography. In the first two imaging modalities the electric field is coupled with magnetic fields of the MRI systems, whereas it is coupled with ultrasound in the last three modalities. More details can be found in [66, 73].

As for any inverse problem, the main issue of coupled physics electrical conductivity imaging is establishing both the uniqueness and stability results. To achieve that, a mathematical model that describes and quantifies the interactions between the physical probing fields needs to be developed. Since one of physical fields is necessarily the electric field, the Maxwell's equations play an important role in such a model. In particular, if the electric field is generated by the surface dc-currents or ac-currents at low frequency, then Maxwell's equations can be reduced to the conductivity equation inside a conductive object with an appropriate boundary condition(s). Due to Ohm's law $\mathbf{J} = -\sigma\nabla u$, the conductivity σ can be expressed as the ratio of magnitudes of the current density $\mathbf{J}$ and ∇u. Substituting this expression in the conductivity equation, one may obtain the nonlinear differential equation subject to the corresponding boundary conditions(s), which serves as a mathematical model of current density imaging.

$$\nabla \cdot (\frac{|\mathbf{J}|}{|\nabla u|}\nabla u) = 0. \tag{1}$$

Moreover, one may generalize such a model by considering the so-called weighted p-Laplace equation

$$\nabla \cdot (\frac{F(x)}{|\nabla u|^{2-p}}\nabla u) = 0,\ 0 \leq p < \infty, \tag{2}$$

which is, in turn, the generalization of the p-Laplace equation (see, e.g., [47]). Here, $F(x) = \sigma(x)|\nabla u|^p$ is the functional mentioned above. Note that in current density imaging, $p = 1$, $F(x) = |\mathbf{J}(x)|$, and the Dirichlet problem for the equation (2) becomes singular and degenerate elliptic. In power density imaging, $p = 0$, $F(x) = \sigma|\nabla u|^2$, and the Cauchy problem for the equation (2) becomes hyperbolic (see, e.g., [9], [39]). This shows that analysis of (2) is a challenging problem.

Note that for $1 \leq p < \infty$ the equation (2) is the Euler-Lagrange equation for the functional

$$M[u] = \int_\Omega F(x)|\nabla u(x)|^p dx,\ u \in H^1(\Omega). \tag{3}$$

However, for $1 < p < \infty$ this functional is strictly convex, whereas for $p = 1$ is only convex, and the convexity is completely lost for $p < 1$. Moreover, for $p = 0$ the form is not valid. Nevertheless, this fact allows for the variational formulation of

coupled physics electrical conductivity imaging, which is well suited for constructing the computational algorithms.

The paper is organized as follows. In the following section, we outline two coupled imaging modalities: EIT and Magnetic Resonance Imaging (MRI) and EIT and Ulrasound Imaging. In Section 3, we survey some mathematical aspects of coupled physics electrical conductivity imaging. Section 4 describes some computational algorithms developed by now to provide recovering the electrical conductivity from the interior data. The effectiveness of these algorithms is demonstrated in computational experiments with simulated data.

2 Some Coupled Imaging Modalities

2.1 MRI+EIT

It is well known that three different types of magnetic fields are utilized in a traditional MRI system. These are the strong static (dc) magnetic field $\mathbf{H}_0$, the so-called gradient field $\mathbf{H}_g$ and the RF field $\mathbf{H}_{RF}$ at the Larmor frequency. So that, in a typical pulse sequence produced by the MRI system the following superposition of magnetic fields is applied at every point x of a bounded domain Ω

$$\mathbf{H}(x) = \mathbf{H}_0(x) + \mathbf{H}_g(x) + \mathbf{H}_{RF}(x).$$

After applying such a sequence, the Free Induction Decay (FID) signal proportional the nuclear magnetisation is then measured and used to produce a magnetic resonance image.

In the traditional EIT imaging modality (see, e.g., [18,23]), the dc or low frequency ($\leq$ 1 kHz) current is injected into the domain Ω from its boundary through surface electrodes. If the domain Ω is filled with a conductive medium, then an additional magnetic field is generated in Ω due to the Bio-Savart law

$$\mathbf{H}_{BS}(x) = \frac{1}{4\pi}\int_{\Omega} \mathbf{J}(y) \times \frac{y-x}{|x-y]^3} dy + a\ harmonic\ function, \quad x \in \Omega,$$

where $\mathbf{J}(x)$ is the current density in Ω generated by the injected current.

Coupling these modalities results in the total magnetic field

$$\mathbf{H}(x) = \mathbf{H}_0(x) + \mathbf{H}_g(x) + \mathbf{H}_{RF}(x) + \mathbf{H}_{BS}(x)$$

generated in Ω, so that the FID signal becomes sensitive to variations of the Bio-Savart field. Thus, the idea is to recover the Bio-Savart field $\mathbf{H}_{BS}$ in Ω from the perturbed FID signals. Such an idea was experimentally realized in [60] as follows.

Let the static magnetic field $\mathbf{H}_0$ be oriented along the z-axis. After injecting a dc or low frequency currents, the Bio-Savart field $\mathbf{H}_{BS}$ produces a phase change in the rotating transverse components (i.e., for $z = z_0$) of the Fourier transforms of the FID signals. Then the imaginary parts M^+ and M^- of such complex valued transforms are given by

$$M^s(x, y, z_0) = M(x, y, z_0)e^{(s)i\mu_0\mu H_z(x,y,z_0)T + i\phi_0},$$

where ϕ_0 is the phase due to the "initial" magnetic field, i.e., without the Bio-Savart field, T is the duration of the surface currents, γ is the gyromagnetic ratio, μ_0, μ are the absolute and relative magnetic permeabilities, and $s = +$ or $-$. Then the measured phase change due to the Bio-Savart field is given by

$$\Psi(x, y, z_0) = \Im \log \frac{M^+(x, y, z_0)}{M^-(x, y, z_0)},$$

where $\Im \log$ means the analytic branch of the complex logarithm. Since $\Psi = 2\gamma\mu_0\mu T H_z$, we obtain

$$H_z = \frac{1}{2\gamma\mu_0\mu T}\Psi.$$

Rotating an object around the vector field $\mathbf{H}_0$ and repeating this process, one may obtain two other components H_x, H_y.

2.1.1 MREIT

In practice, one can measure only one component of the Bio-Savart field if an object is positioned along the vector field $\mathbf{H}_0$. To measure the other components, the object needs to be rotated around it. The detailed description of the physical principles of MREIT can be found in the review papers [66,67]. Since such a rotation is problematic in a commercial MRI system, it may seem that the following inverse model formalizes Magnetic Resonance Electrical Impedance Tomography (MREIT).

Given (H_z, g), where H_z is the z-component of the Bio-Savart field in Ω resulted from injecting the dc or low frequency current through $\partial\Omega$, and the functions $\sigma(x)$ and $g(x)$ are related to the voltage potential $u(x)$ by

$$\nabla \cdot (\sigma \nabla u) = 0 \text{ in } \Omega \subset R^3, \tag{4}$$

$$\partial_n u = g \text{ on } \partial\Omega, \tag{5}$$

find the electrical conductivity σ in Ω. However, knowledge of only one pair (H_z, g) is not enough to guarantee the unique reconstruction. It was shown in [64,65] that in two dimensions the uniqueness result can be established if two z-components H_{z1} and H_{z2} of two linearly independent Bio-Savart fields resulted from applying two surface currents are measured. However, it still remains unclear whether this result may be extended to three dimensions. It should also be mentioned that although there is available in the mathematics literature (see, e.g., [66]) a number of MREIT techniques used in both the numerical and biomedical experiments, the convergence result was established only for few specific cases (see [48]). It was recently shown (see [62]) that in MREIT at the Larmor frequency one can determine the field $H_x + iH_y$ inside (where both components H_x, and H_y are complex valued). Moreover, under further axial assumptions, one can determine the isotropic conductivity.

2.1.2 CDI

In the mathematics literature the term Current Density Imaging (CDI) (or Current Density Impedance Imaging (CDII)) is associated with the group of imaging techniques

exploiting a coupled imaging modality in which an MRI system is normally, but not necessarily, uzed to recover the electrical conductivity σ in Ω from the current density $\mathbf{J}$ or its functionals. If an object is rotated around the vector field $\mathbf{H}_0$, then all components of the Bio-Savart field can be measured, so that the vector field $\mathbf{H}_{BS}$ is determined. Due to Ampere's law, the current density $\mathbf{J}$ generated by the surface current electrodes inside Ω can then be determined as

$$\mathbf{J} = \nabla \times \mathbf{H}_{BS}.$$

This relation was exploited in the first CDI modality (see [60, 61]).

It is well known that in a linear conductive medium the Ohm's law takes place

$$\mathbf{J} = -\sigma \nabla u. \tag{6}$$

This relation is the physical basis of all existing CDI techniques. It should also be mentioned that since both quantities $\sigma(x)$ and $u(x)$ are unknown in Ω, an inverse conductivity problem is inherently nonlinear. Although there are several formulations of the inverse conductivity problem, as well as approaches to its solution, the common feature is, however, that the electric conductivity relates to the voltage potential by (4) in case of the static or low frequency electromagnetic field and isotropic conductivity.

In [41] the following problem was considered. Given a single measurement $(\mathbf{J}, f)$, where f is the trace of the voltage potential on the boundary $\partial\Omega$, find σ in Ω. In 2D, the unique recovery σ from $(\mathbf{J}, f)$ was based on the fact that the vector field $\mathbf{J}$ is normal to equipotential lines. In [KKS1] the relation (6) was used to reduce the conductivity equation (4) to the degenerate elliptic equation

$$\nabla \dot{(} \frac{|\mathbf{J}|}{|\nabla u|} \nabla u) = 0 \text{ in } \Omega \tag{7}$$

and it was shown that knowledge of the applied current at the boundary $\partial\Omega$ together with the magnitude of current density field $|\mathbf{J}|$ inside Ω is insufficient for the unique reconstruction of σ. To overcome this difficulty, the so-called J- substitution algorithm was proposed. It was shown in [36] that applying two surface currents and using magnitudes of two linearly-independent current density fields $(|\mathbf{J}_1|, |\mathbf{J}_2|)$ provides the unique and stable recovery of σ. In [JNH] an explicit reconstruction formula for $\nabla \ln \sigma(x)$ was derived for the case when two transversal current density fields are available. Later, the same expression was independently discovered in [46].

Observing the imaging techniques indicated above, one may notice that the current density vector field(s) together with the boundary currents or voltage potentials are required to reconstruct the electrical conductivity. However, the presence of only one magnitude of the current density in (7) motivates the formulations of the CDI problem with a single measurement of boundary and interior data. In [56] such formulations were proposed and analized for the first time. In [56] it was shown that knowledge of only one $\mathbf{J}$ in Ω together with the Cauchy data on a part of $\partial\Omega$ provides the global uniqueness and conditional stability results.

2.2 Coupling the EIT and Ultrasound Imaging Modalities

The main idea is that such a combination may possess the high contrast resolution, which is typical for the EIT imaging modality, as well as the high spatial resolution, which is provided by the ultrasound imaging modality. However, the practical realization of this idea can be based on different physical phenomena that we consider below.

Resulted from applying the standard EIT setting to a conductive medium, the distributions of both quantities $\mathbf{E}$ and $\mathbf{J}$ yield the distribution of the electrical energy in Ω. The latter is given by Joule's law as $W = \mathbf{J} \cdot \mathbf{E}$. The energy is spent on raising temperature in the medium thereby creating a pressure wave, which is recorded on $\partial\Omega$. This phenomenon was utilized in [28] when constructing the forward and inverse mathematical models. Specifically, the process of propagation and scattering of the pressure wave was modelled by the Cauchy problem for the wave equation

$$\partial_{tt} p - c^{-2}(x)\nabla^2 p = 0 \ \text{ in } R^3 \times (0, \infty), \tag{8}$$

$$p(x, 0) = p_0, \quad \partial_n p(x, 0) = 0 \ \text{ in } R^3. \tag{9}$$

Measuring the boundary pressure, i.e., $p(x, t), x \in \partial\Omega$, one may then determine the initial condition $p_0(x)$. Although by itself, this problem is of great interest, it is out of scope of our survey.

Assuming that the boundary pressure is proportional to the Joule's energy, i.e., $p_0(x) = \gamma(\mathbf{J} \cdot \mathbf{E})$, one may obtain the interior data

$$W(x) = \frac{p_0(x)}{\gamma}$$

and formulate the inverse problem is follows. Given (f, g, W), where $f = u(x)$, $g = \partial_n u(x)$, $x \in \partial\Omega$, and the voltage potential $u(x)$ satisfies the equation (4), find $\sigma(x)$ in Ω. Using multiple data, the uniqueness result was established in [22] (in 2D) and [8] (in 3D). The stability was studied in [40].

In the other implementation (see [4], a conductive medium is perturbed by focusing ultrasonic waves on a sufficiently small volume of the object to be investigated. Such mechanical perturbations lead to elastic deformations of the medium that, in turn, cause variations of conductivity. Then the focus of ultrasound waves scans the entire domain, and the variations of the voltage potential are sensed by the standard EIT settings on the boundary $\partial\Omega$. Analogously, the measured changes of the boundary voltage potential can be used to determine the power density $W(x)$ in Ω.

3 Some Mathematical Aspects

It was shown in the previous section that in both CDI and Ultrasound EIT the interior data is represented by functionals of $\nabla(u)$. But in CDI it has the form $F(x) = \sigma(x)|\nabla u(x)|$, whereas in Ultrasound EIT it takes the form $F(x) = \sigma(x)|\nabla u(x)|^2$. Then substituting these functionals in the conductivity equation

$$\nabla \cdot (\sigma(x)\nabla u(x)) = 0, \tag{10}$$

one obtain two nonlinear PDEs

$$\nabla \cdot (\frac{F(x)}{|\nabla u|}\nabla u) = 0 \tag{11}$$

or

$$\nabla \cdot (\frac{F(x)}{|\nabla u|^2}\nabla u) = 0. \tag{12}$$

This fact gives rise to the analogy with the p-Laplace equations. It follows from the classical theory (see, e.g., [27,47]) that the Laplace equation is the Euler-Lagrange for the Dirichlet integral

$$\int_\Omega |\nabla u|^2 dx.$$

Let $p \geq 0$ be a real number. Consider the integral

$$\int_\Omega |\nabla u|^p dx.$$

Then the nonlinear PDE

$$\nabla \cdot (|\nabla u|^{p-2}\nabla u) = 0$$

is the corresponding Euler-Lagrange equation. Such an equation is called the p-Laplace equation. A natural generalization of both (11) and (12) can be written as the weighted p-Laplace equation

$$\nabla \cdot (\frac{F(x)}{|\nabla u|^{2-p}}\nabla u) = 0. \tag{13}$$

If $1 \leq p < \infty$, then (13) is the Euler-Laplace equation for the functional

$$M[u] = \int_\Omega F(x)|\nabla u|^p dx. \tag{14}$$

If $1 < p < \infty$, then the weighted p-Laplace equation is elliptic, and the functional $M[u]$ is strictly convex, so that it has a unique minimizer. If $p = 1$, the equation is degenerate elliptic, and the functional is convex, but not strictly convex. Finally, if $p < 1$, the weighted p-Laplace equation becomes hyperbolic, and the functional $M[u]$ loses convexity. For $p = 0$ the functional (14) must be replaced with

$$M[u] = \int_\Omega F(x) \ln |\nabla u| dx.$$

Thus, the coupled physics inverse conductivity problem can be formulated as follows. Find the pair $(u(x), \sigma(x))$, $x \in \Omega$, where the quantities $u(x)$ and σ are related by (13), given the interior $F(x)$ and appropriate boundary condition(s). Depending on how many "measurements" of the interior and boundary data is used, we will distinct between the inverse problems with the single or multiple measurements. A single measurement means that the data associates with only minimal information, i.e., with only one $F(x)$ and one set of boundary data.

We state one general result demonstrating the close connection of a coupled physics electrical conductivity imaging with the classical differential geometry. Let $\Omega \subset R^n$ be

an open set with the conformal metric $g = |J|^{2/(n-1)}I$, where $|\nabla u| > 0$. Recall that any solution $u \in H^1(\Omega)$ to the conductivity equation (10) is said to be a σ-harmonic function. Then the following theorem takes place.

Theorem 1[NNT1] *Let $u \in C^1(\Omega)$ be a σ-harmonic function. Then the level sets $u = c$ are surfaces of zero mean curvature*

$$H = |J|^{n/(1-n)} \nabla \cdot (|J| \frac{\nabla u}{|\nabla u|})$$

in the conformal metric g. Moreover, they are critical surfaces for the functional

$$\int_\Sigma |\mathbf{J}| dS,$$

where $\Sigma = \{x \in \Omega : u = c\}$, and dS is the Euclidean surface measure.

In two dimensions, the equipotential lines are also geodesics in the conformal metric, and they can be viewed as characteristics of (11). One may, therefore, find the geodesics originating on the part of the boundary where measurements are available, and the voltage potential $u(x)$ is then determined in the region spanned by these characteristics.

3.1 The Interior and Cauchy Data

If the conductivity $\sigma(x)$ is supposed to be known on the boundary $\partial\Omega$ (or on a part of it), then it is meaningful to pose both the Dirichlet and Neumann conditions.

3.1.1 A Single Measurement

The Weighted 1-Laplace Equation. Consider the following inverse problem.

Given the Cauchy data $(u, \partial_n u)$ on a part Γ of the boundary and the magnitude of the current density $|\mathbf{J}|$ in Ω, find the conductivity σ in Ω.

Let Ω be a simply connected planar domain with the sufficiently smooth boundary $\partial\Omega$, and $\sigma \in L^\infty(\Omega)$ be a positive function. A map on the connected boundary of such a domain is said to be two-to-one if the set of local maxima is either one point or one connected arc. Let f be a continuous function on a simple closed curve. It is said to be almost two-to-one if it is a two-to-one map, except possibly at its extrema. It was shown in [AL3] that if the trace $u_{|\partial\Omega}$ of a σ-harmonic function u in Ω is almost two-to-one, then $|\nabla u| > 0$ in Ω, and each level set of u is a sufficiently smooth curve inside Ω whose endpoints lie on $\partial\Omega$.

Theorem 2[NTT1] (Uniqueness) *Let $f \in C^2(\partial\Omega)$ be an almost two-to-one function and Γ be a maximal arc on which f is strictly monotone. Then for $|\mathbf{J}| \in C^1(\overline{\Omega}) \cap C^2(\Omega)$ and $g \in C^1(\Gamma)$, there exists a unique pair $(\sigma, u) \in C^2(\Omega) \times C^2(\Omega)$, such that u is σ-harmonic in Ω and $u = f$, $\partial_n u = g$ on Γ.*

It follows from this theorem that if a part of Ω is not spanned by the characteristics originated on Γ, then uniqueness cannot be established. An example of non-uniqueness can be found in [NTT1] (see Proposition 3.1).

Let u, u_1 be two admissible σ, σ_1-harmonic maps, such that $u_{|\Gamma} = f$, $u_{1|\Gamma} = f_1$, $\partial u_{|\Gamma} = g$, $\partial u_{1|\Gamma} = g_2$, $|\mathbf{J}| = \sigma|\nabla u|$, $|\mathbf{J}_1| = \sigma_1|\nabla u_1|$. Denote $\|u\|_{C^1(\overline{\Omega})} = \|u\|_\infty + \|\nabla u\|_\infty$.

Under such assumptions, the following result takes place.

Theorem 3[NTT1] (Stability) *Let $f, f_1 \in C^2(\partial\Omega)$ be almost two-to-one maps that have a common maximal arc Γ and such that $\inf_\Gamma f \geq \varepsilon, \inf_\Gamma f_1 \geq \varepsilon$, $\max\{\|g/f^{'} - g_1/f_1^{'}\|_{C^1(\Gamma)}, \|f^{-1} - f_1^{-1}\|_{C^1(\Gamma)}, \|\nabla(\ln|\mathbf{J}| - \ln|\mathbf{J}_1|)\|_{C^1(\Gamma)}\}$ $\leq \delta$ for some $\delta > 0$. Then*

$$\|\sigma - \sigma_1\|_\infty \leq \varphi(\delta),$$

where $\varphi : [0,\infty) \to [0,\infty)$ is a map depending on $\varepsilon, \|\sigma_1\|_\infty, \|g_1/f_1^{'}\|_\infty$, and $\|f_1^{-1}\|_\infty$, such that $\varphi(\delta) \to 0$ as $\delta \to 0$.

Note that since the estimate $\varphi(\delta)$ depends on $\|\sigma_1\|_\infty$, the stability is conditional.

The Weighted 0-Laplace Equation. Consider the following inverse problem.

Given the Cauchy data $(u, \partial_n u)$ on $\partial\Gamma$ and the power density $W(x) = \sigma(x)|\nabla u|^2$ in Ω, find the conductivity σ in Ω.

Clearly, in this case the inverse model is represented by the Cauchy problem for the nonlinear PDE (12). Unlike the previous case, this problem is hyperbolic. This can easily be seen after transforming the Cauchy problem to the form (see also [BalC])

$$\eta^{ij}(\nabla u)\partial_{ij}^2 u + k^i \partial_i u = 0, \quad \text{in } \Omega,$$

$$u = f, \quad \partial_n u = g \quad \text{on } \partial\Omega,$$

where $k^i = -\nabla \ln W$, (η^{ij}) is a definite matrix of signature $(1, n-1)$. In [9] the local uniqueness and stability results (see Theorem 3.1) were established on a domain of influence of the space-like part of the boundary swept out by the space-like surfaces. It should be mentioned that the local uniqueness and stability results can also be established from the general theory of ill-posed problems for PDEs [45]. Note that if Ω is the geometry with a hole, i.e., an annulus, in 2D, it and $\sigma(x)$ are sufficiently smooth, and $|\nabla u|$ is bounded, then Theorem 3.1 provides the global results (see [9], Section 4.1).

3.1.2 Multiple Measurements

Utilizing the concept of complex Geometric Optics Solutions (CGOs) and three interior measurements, the global uniqueness and stability results were established for $n \geq 2$ (see [9], Section 4.2). Specifically, under an assumption that $\sigma(x)$ can be extended by $\sigma_0 = 1$ on $R^n \backslash \Omega$ and it is smooth on R^n, it was shown in [9] (see Theorem 4.5 for detail) that there exists an open set of functions $\{f_1, f_2\}$ on $\partial\Omega$, such that if u_1 and u_2 are the corresponding solutions to the conductivity equation (10), then the measurements

$$W_1 = \sigma(x)|\nabla u_1|^2, \; W_2 = \sigma(x)|\nabla u_2|^2, \; W_3 = \sigma(x)|\nabla(u_1 + u_2)|^2$$

together with the corresponding Cauchy conditions $(f_1, g_1), (f_2, g_2), (f_1 + f_2, g_1 + g_2)$ uniquely determine $\sigma(x)$ in a domain defined by CGOs. Moreover, if $W_{ij}, \hat{W}_{ij}$ and $(f_1, g_1), (f_2, g_2)$ and $(\hat{f}_1, \hat{g}_1), (\hat{f}_2, \hat{g}_2)$ are the interior and Cauchy data corresponding to σ and $\hat{\sigma}$ and if the norms of $\sigma(x) - 1$ and $\hat{\sigma}(x) - 1$ are bounded by M in $H^{n/2+3+\varepsilon}$ for some $\varepsilon > 0$, then there exists the constant $C = C(M)$, then the global stability result takes place

$$\|\sigma - \hat{\sigma}\| \leq C(\|\gamma - \hat{\gamma}\| + \sum_{(i,j)\in S} \|\nabla W_{ij} - \nabla \hat{W}_{ij}\|),$$

where $S = \{(1,1),(1,2),(2,2)\}$, $\gamma = (f_1, g_1, f_2, g_2), \hat{\gamma} = (\hat{f}_1, \hat{g}_1, \hat{f}_2, \hat{g}_2)$, and $\|\cdot\|$ is the L_2-norm on the corresponding sets.

Note that if a finite set of measurements

$$W_{ij} = \sigma(x)\nabla u_i \cdot \nabla u_j, \quad (i,j = 1,2,...,M)$$

is available in Ω for $M = n$, n is even or for $M = n+1$, n is odd, then the global result can be formally obtained without knowledge of the corresponding Cauchy data (see [10], Section 4.2).

3.2 The Interior and Dirichlet Data

Consider the weighted 1-Laplace equation (11). It was shown in [35] that knowledge of the pair $(|\mathbf{J}|, g)$, where $g = \sigma\partial_n u(x), x \in \partial\Omega$, is insufficient in order to establish existence and uniqueness. The alternative is either to acquire two magnitudes of the current density in Ω corresponding to two different surface currents or to use a single measurement of $|\mathbf{J}|$ together with the Dirichlet condition on $\partial\Omega$. However, in the latter case existence of the so-called viscosity solutions (see the notion in [24]) may prevent uniqueness as well. In [SZ] it was shown that for $|\mathbf{J}| \equiv 1$ in $\Omega = \{(x_1, x_2) \in R^2 : x_1^2 + x_2^2 < 1\}$ and $f = x_1^2 - x_2^2$ on $\partial\Omega$ there exist a parametric family of viscosity solutions

$$u_t(x_1,x_2) = \begin{cases} \{2x_1^2 - 1, if|x_1| \geq \sqrt{\frac{1+t}{2}}, |x_2| \leq \sqrt{\frac{1-t}{2}} & \\ t, & if|x_1| \leq \sqrt{\frac{1+t}{2}}, |x_2| \leq \sqrt{\frac{1-t}{2}} \\ 1 - 2x_2^2, & if|x_1| \leq \sqrt{\frac{1+t}{2}}, |x_2| \geq \sqrt{\frac{1-t}{2}} \end{cases}$$

where $t \in [-1,1]$. We observe that the only solution $u_0(x), x = (x_1, x_2)$ is a minimizer of the functional

$$M[v] = \int_\Omega |\mathbf{J}(x)||\nabla u(x)|dx \tag{15}$$

with the constraint $v = f$ on Ω over the space of functions with bounded variations. This fact motivates minimizing the functional $M[z]$ instead solving the Dirichlet problem for the weighted 1-Laplace equation. At the same time, this example shows that if one minimize $M[z]$ for an arbitrary data $(|\mathbf{J}|, f)$, then it is possible to obtain solutions $u(x)$, such that $\nabla u = 0$ on open sets while $|\mathbf{J}| \equiv 1$ in Ω. Clearly, such solutions are extraneous since they do not represent voltage potentials. Therefore, the concept of the admissible data needs to exploited in order to exclude extraneous solutions. In particular (see [NTT2]), a pair $(|\mathbf{J}|, f)$ is called admissible if for every pair $(|\mathbf{J}|, f) \in L_2(\Omega) \times H^{1/2}(\partial\Omega)$ there exists a function $\sigma(x) \in L_+^\infty$. such that $\sigma|\nabla u| = |\mathbf{J}|$, where $u \in H^1(\Omega)$ is a weak solution to the Dirichlet problem for the weighted 1-Laplace equation. Clearly, the pair $(1, x_1^2 - x_2^2)$ is the example indicated above is not admissible since $\sigma|\nabla u| \neq |\mathbf{J}|$ in the square $[-1/\sqrt{2}, 1/\sqrt{2}] \times [-1/\sqrt{2}, 1/\sqrt{2}]$. The following uniqueness result takes place

Theorem 4[NTT2] *Let $\Omega \subset R^n, n \geq 2$ be a domain with the $C^{1,\alpha}$-boundary, $(|\mathbf{J}|, f) \in C^\alpha(\overline{\Omega}) \times C^{1,\alpha}(\partial\Omega)$ be an admissible pair, and $\sigma \in C^\alpha(\overline{\Omega})$. If $|\mathbf{J}| > 0$ almost everywhere*

in Ω*, then the variational problem*

$$argmin\{M[v] : v \in W_+^{1,1}(\Omega) \sqcap C(\Omega), u_{|\partial\Omega} = f\}, \tag{16}$$

where $W_+^{1,1}(\Omega) = \{u \in L_1(\Omega) : \nabla u \in L_1(\Omega)\}$*, has a unique solution* u *and* $\sigma = |\mathbf{J}|/|\nabla u|$.

If $n = 2$, then for a simply connected planar domain the sufficient condition formulated in Theorem 4 can be simplified as follows

Theorem 5[NTT2] *Let* $\Omega \subset R^2$ *be a simply connected domain with the* $C^{1,\alpha}$*-boundary,* $(|\mathbf{J}|, f) \in C^{\alpha}(\overline{\Omega}) \times C^{1,\alpha}(\partial\Omega)$ *be an admissible pair with the almost two-to-one function* f*, then there exists a unique* $\sigma > 0$ *in* $C^{\alpha}(\overline{\Omega})$*, such that* $|\mathbf{J}| = \sigma|\nabla u|$*, where* u *is the solution of the variational problem (16).*

In [53] the uniqueness result (see Theorem 4) was extended to the weighted least gradient problem in the space of functions with bounded variations, $BV(\Omega)$, i.e., to the problem

$$\text{argmin}\{\int_{\Omega} a(x)|Dv| : v \in BV(\Omega), v_{|\partial\Omega} = f\}, \tag{17}$$

where the function $a(x) \in C^{\alpha}(\Omega)$ is allowed to be vanished on some sets. In [JMN] the variational problem (17) was extended to the general least gradient problem

$$\text{arginf}\{\int_{\Omega} \varphi(x, Dv) : v \in BV_f(\Omega)\}, \tag{18}$$

where $BV_f(\Omega) = \{v \in BV(\Omega) : \forall x \in \partial\Omega, \lim_{y\in\Omega, |x-y|<r} |f(x) - v(y)| = 0\}$, $f \in C(\partial\Omega)$, and $\varphi(x, \xi)$ is a function that is convex and homogeneous of degree 1 with respect to the ξ-variable, so that the functional in (18) is the total variation of u in Ω. Note that for $\varphi(x, \xi) = a(x)|\xi|$ the variational problem (18 is reduced to the problem (17), and if $a(x) = |\mathbf{J}(x)|$, then we obtain (16).

Suppose the function $\varphi(x, \xi)$ satisfies the following conditions.

(1) $\exists\alpha > 0 : \alpha|\xi| \le \varphi(x, \xi) \le \alpha^{-1}|\xi|, \forall x \in \Omega \wedge \xi \in R^n$;

(2) the map $\xi \to \varphi(x, \xi)$ is a norm $\forall x$;

(3) $\varphi \in W_{loc}^{2,\infty}$ away from $\xi = 0$ and $\exists C > 0 : \varphi_{\xi_i\xi_j}(x, \xi)p^i p^j \ge C|p^{'}|^2$, $\forall \xi \in S^{n-1} \wedge\ p \in R^n$, where $p^{'} = p - (p \cdot \xi)\xi$;

(4) φ and $D_\xi\varphi$ are $W^{2,\infty}$ away from $\xi = 0$ and $\exists\rho = const > 0, \lambda = const > 0$: $\varphi(x, \xi) + |D_\xi\varphi(x, \xi)| + |D_\xi^2\varphi(x, \xi)| + |D_\xi^3\varphi(x, \xi)| + \rho|D_x D_\xi\varphi(x, \xi)| + \rho|D_x D_\xi^2\varphi(x, \xi)| + \rho^2|D_x^2 D_\xi\varphi(x, \xi)| \le \lambda$, $\forall x \in \Omega, \xi \in S^{n-1}$.

Then the following results take place.

Theorem 6[JMN](Existence) *Let* $\varphi : R^n \times R^n \to R$ *be a continuous function that satisfies conditions (1)-(2), and* $\Omega \subset R^n$ *be a bounded Lipschitz domain. If* Ω *satisfies the barrier condition with respect to* φ*, i.e.,* $\partial\Omega$ *satisfies a positivity condition on a sort of generalized mean curvature related to* φ*, then* $\forall f \in C(\partial\Omega)$*there exists a solution of the problem (18) in* $BV_f(\Omega)$.

Theorem 7[JMN](Uniqueness and stability) *Let* $\Omega \subset R^n$ *be a bounded Lipschitz domain with the connected boundary, and* $\varphi : \Omega \times R^n \to R$ *satisfies conditions (1)-(4). Suppose* u_1, u_2 *are solutions of (18) in* $BV_{f_1}(\Omega), BV_{f_2}(\Omega)$ *for* $f_1, f_2 \in C(\Omega)$*. Then*

$$|u_1 - u_2| \le \sup_{\partial\Omega} |f_1 - f_2| \ \textit{a.e. in}\ \Omega.$$

Moreover,

$$u_2 \geq u_1 \ \textit{a.e. in } \Omega \ \textit{if } f_2 \geq f_1 \ \textit{on } \partial\Omega.$$

In particular, $\forall f \in C(\partial\Omega)$ *there exists at most one solution of the problem (18) in* $BV_f(\Omega)$.

The results indicated above were obtained under an assumption that the conductivity $\sigma(x)$ is isotropic in Ω. Recently, they were extended to an anisotropic conductivity matrix in a known conformal class from one interior measurement (see [30]). Specifically, the matrix valued conductivity was represented in the form

$$\sigma(x) = c(x)\sigma_0(x), \tag{19}$$

where $c(x) \in C^\alpha$ is a positive scalar valued function and $\sigma_0(x) \in C^\alpha \cap\ C^\alpha$ $(\Omega, Mat(n, R^n))$ is a given positive definite symmetric matrix valued function, which can be determined from Diffusion Tensor Magnetic Resonance Imaging (see [49]). Under these conditions, the following analogue of Theorem 7 takes place.

Theorem 8[HMN] *Let* $\Omega \subset R^n$ *be a bounded Lipschitz domain with the connected boundary, and assume that*

$$\varphi(x,\xi) = a(x)\sqrt{\sum_{i,j=1}^{n} \sigma_0^{ij}(x)\xi_i\xi_j},$$

where $a(x) \in C^{1,1}(\Omega)$ *is positive and bounded away from zero and* $\sigma_0(x) \in C^{1,1}(, Mat(n, R^n))$ *satisfies*

$$m|\xi|^2 \leq \sum_{i,j=1}^{n} \sigma_0^{ij}(x)\xi_i\xi_j \leq M|\xi|^2, \ \forall \xi \in R^n$$

for some $0 < m, M < \infty$. *If* $u1, u2 \in BV(\Omega)$ *are solutions of the variational problem (18) in* $BV_{f_1}(\Omega), BV_{f_2}(\Omega)$ *respectively, with* $f_1, f_2 \in C(\partial\Omega)$ *, then*

$$|u_2 - u_1| = \sup_{\partial\Omega} |f_2 - f_1| \ \textit{a.e. in } \Omega.$$

Morever, $u_2 \geq u_1$ *a.e. in* Ω *if* $f_2 \geq f_1$ *on* $\partial\Omega$. *In particular, for the class of* φ *as described above, (18) has at most one minimizer in* $BV_f(\Omega)$, *and any minimizer is continuous if* $n = 3$.

In [14–16] it was recently shown that if a minimum number of $(n + 2)$ of internal current densities **J** is available, the uniqueness result can also be established for a more general anisotropic conductivity, i.e., without the assumption (19).

In studying the coupled physics inverse conductivity problem, the stability issue is of particular interest to researchers. Indeed, utilizing the interior data, one may expect a much better behaviour of the modulo of continuity of a map generated by this problem. However, due to the nonlinearity, obtaining some estimates of this function is a challenging problem. Up to now, just few stability results are available in the mathematics literature. In [40], a formal linearization was derived by considering small perturbations of the isotropic conductivity $\sigma(x)$. The stability of the linearized problem with one (for $0 < p < 1$) or two (for $1 \leq p \leq 2$) interior data was then

proved. In [MS] for one interior data $F(x) = \sigma|\nabla u|^p$the stability was first proved for the linearization, and it was then used to establsih the stability result for the nonlinear problem. Specifically, such a result was formulated as follows.

Theorem 9[MS] *Let $0 < p \leq 1$ and u_0 be σ_0-harmonic, such that $\nabla u_0 \neq 0$ in $\overline{\Omega}$. Then $\forall \theta \in (0,1) \exists s > 0$, such that if $\|\sigma\|_{H^s(\Omega)} < L, L > 0, \exists \varepsilon > 0$, such that $\|\sigma - \sigma_0\|_{C^2(\Omega)} < \varepsilon$ then $\|\sigma - \sigma_0\|_{L_2(\Omega)} < C\|F[\sigma] - F[\sigma_0]\|^{\theta}_{L_2(\Omega)}$.*

4 Computational Algorithms

To construct computational algorithms for coupled physics conductivity imaging, one may try either to solve numerically the nonlinear equation (13) with the Cauchy or Dirichlet condition or to construct some minimizing sequences for the functional (14). Then, one may exploit the Ohm's law $\mathbf{J} = \sigma\mathbf{E}$ in order to find the conductivity σ. Below, we outline some realizations of this approach.

4.1 Reconstruction of level sets of the voltage potential

Apparently, the first computational algorithm for solving the coupled physics inverse conductivity problem was proposed in [41]. It exploits the fact that in two dimensions the vector $\mathbf{J}$ is normal to equipotential lines at every point in Ω. Specifically, since the unit vector $\mathbf{J}/|\mathbf{J}| = \nabla u/|\nabla u| = \mathbf{e}$ is orthogonal to an equipotential line $L(t) : (x(t), y(t))$ at every point, where t is a parameter, then all the equipotential lines can be reconstructed by solving the ODE $L^{'}(t) = \mathbf{e}^{\perp}$ in Ω, $u = f$ on $\partial\Omega$. Here, $(\cdot)^{\perp}$ is the operator of the right-angle counterclockwise rotation. It is assumed that $|\mathbf{J}| \neq 0$ everywhere in Ω. Clearly, this algorithm inherits all advantages and disadvantages that are typical for the numerical methods for the first order ODEs.

In contrast, the algorithm proposed in [56] utilizes the magnitude of the current density $|\mathbf{J}|$ together with the Cauchy data on a part $\Gamma$of $\partial\Omega$. The equipotential lines are recovered from the Cauchy boundary value problems for the system of the second order ODEs

$$x_{tt} = -x_t^2 \frac{|\mathbf{J}|_x}{|\mathbf{J}|}(x,y) - 2x_t y_t \frac{|\mathbf{J}|_y}{|\mathbf{J}|}(x.y) + y_t^2 \frac{|\mathbf{J}|_x}{|\mathbf{J}|}(x,y), \tag{20}$$

$$y_{tt} = -x_t^2 \frac{|\mathbf{J}|_y}{|\mathbf{J}|}(x,y) - 2x_t y_t \frac{|\mathbf{J}|_x}{|\mathbf{J}|}(x.y) - y_t^2 \frac{|\mathbf{J}|_y}{|\mathbf{J}|}(x,y), \tag{21}$$

where $(f, |\mathbf{J}|) \in C^{2,\alpha}(\partial\Omega) \times C^{1,\alpha}(\Omega)$. Note that the equipotential lines are originated on the arc Γ of the boundary $\partial\Omega$, so that the conductivity σ is reconstructed in a region spanned by these equipotential lines. The conditional stability of this algorithm follows from Theorem 3. The inversion and stability results are based on classical arguments on the existence and stability of solutions of ordinary differential equations. To demonstrate the computational feasibility of this algorithm, the interior data $|\mathbf{J}|$ in Ω and Cauchy data on a part of $\partial\Omega$ was numerically simulated. We used the same conductivity but the interior data $|\mathbf{J}|$, as well as the Cauchy data, is generated by solving two distinct Dirichlet problems. In one problem the boundary voltage was almost two-to-one, while in the other problem it was not. The equipotential

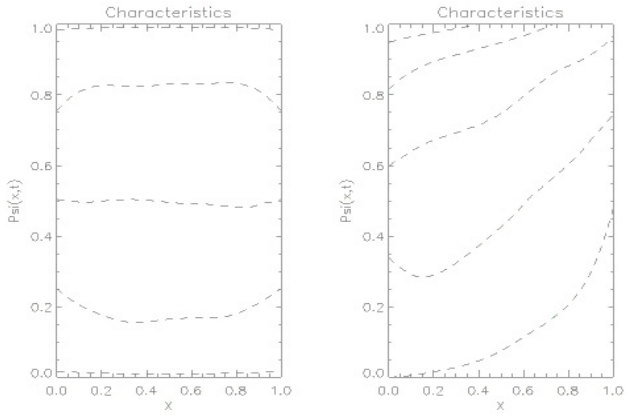

Figure 1: Characteristics computed for the almost two-to-one boundary voltage (left)O and for non two-to-one boundary voltage (right).

Figure 2: The conductivity images reconstructed from the noiseless (left) and noisy (right) data simulated from the non two-to-one boundary voltage.

lines (characteristics) are calculated by solving the system (20)-(21) together with the Cauchy data on the left side of the rectangle.

Figure 1 shows the equipotential lines (characteristics) from the corresponding two experiments. Note that when $|\mathbf{J}|$ is generated by boundary data which does not satisfy the almost two-to-one condition, the equipotential lines originating on the left side of the rectangle do not fill the lower right corner of the rectangle. Figure 2 shows conductivities reconstructed in the experiment with the non two-to-one boundary data. The lower right corner of images shown in this figure demonstrates computational artifacts. They are due to the fact that this region is not covered by characteristics.

Instead the Cauchy data, the Dirichlet data can also be used when solving the system (20)-(21). In this case, the inversion is based on solving two point boundary value problems, and it allows for obtaining geodesics joining pairs of equipotential points at the boundary. While for general manifolds with boundary the system (20)-(21) may not be uniquely solvable, the following uniqueness result takes place.

Figure 3: The conductivity images recovered from partial interior and boundary data.

Theorem 10 [NTT3] *Let $\Omega \subset R^2$ be a simply connected domain with $C^{2,\alpha}$-boundary, $0 < \alpha < 1$. Let $(f, |\mathbf{J}|) \in C^{2,\alpha}(\partial\Omega) \times C^{1,\alpha}(\Omega)$ be an admissible pair with f almost two-to-one and let $(x_0, y_0), (x_1, y_1) \in \partial\Omega$ be such that $f(x_0, y_0) = f(x_1, y_1)$. Then the system (20)-(21) with the boundary conditions*

$$(x(0), y(0)) = (x_0, y_0) \text{ and } (x(1), y(1)) = (x_1, y_1) \tag{22}$$

has a unique solution $\gamma(t) = (x(t), y(t) : [0, 1] \to \Omega$. Moreover, the map $u : \Omega \to R$ is constant along γ, i.e., $(u \circ \gamma)(t) = \lambda, t \in [0, 1]$.

Since the solutions of (20), (21) and (22) depend only on $|\mathbf{J}|$ near an equipotential line, one may perform reconstruction of σ from incomplete interior data. Let $|\mathbf{J}|$ be given in a subregion $\tilde{\Omega}$, such that

$$\Omega_{\alpha,\beta} = \{x \in \overline{\Omega} : \alpha < u(x) < \beta\},$$

where α and β ar unknown. To find an equipotential line lying entirely in $\tilde{\Omega}$, we solve the problem (20), (21) and (22) for each pair of the boundary points. If the solution lies in the interior of $\tilde{\Omega}$, then it is the correct level curve joining those two boundary points. If the calculated line passes outside $\tilde{\Omega}$ (or touches its boundary) then it is dependent on the extension of $|\mathbf{J}|$ and we discard it. An interval (α, β) of voltages defines a set $\Omega_{\alpha,\beta}$ provided that, for each (α, β), the calculated λ-equipotential line lies entirely in the interior of $\tilde{\Omega}$. If $\tilde{\Omega}$ contains no entire equipotential lines, then all the numerical solutions will be discarded. An example of the conductivity reconstruction from the incomplete data is shown in Figure 3. This algorithm provides the local convergence (i.e., an initial approximation is supposed to be close to the sought solution) that cannot be strengthened based on the length minimizing property alone in a general metric space: In the case of a hemisphere, infinitely many geodesics connecting diametral points. In contrast, in the recent paper [TTV], a globally convergent algorithm (in the sense that s solution does not depend on an initial approximation) was proposed. The idea is that the level sets are characteristics of a first-order PDEs. It was shown that the length of these characteristics depend continuously on the boundary points and directions. This is a global geometrical property that requires the convexity of the domain, and uses the fact that the Euclidean curvature of the characteristics are a priori bounded. The

convergence rate of the algorithm depends on the modulus of continuity of lengths of characteristics with respect to the shooting direction.

4.2 A Simple Iterative Procedure

The other method of constructing a minimizing sequence for the functional (14) for $p = 1$ was proposed in [57]. It is based on the following minimization property.

Theorem 11 [NTT2] *Let $v \in H^1(\Omega)$ be such that $|\mathbf{J}|/|\nabla v| \in L^\infty_+(\Omega)$. Let $u \in H^1(\Omega)$ be the weak solution of the problem*

$$\nabla \cdot (\frac{|\mathbf{J}|}{|\nabla v|}\nabla u) = 0, \quad in \ \ \Omega,$$

$$u = v \quad on \ \ \partial\Omega.$$

Then the following inequalities hold

$$\int_\Omega |\mathbf{J}||\nabla u|dx \leq \int_\Omega |\mathbf{J}||\nabla v|dx, \tag{23}$$

$$\int_\Omega |\mathbf{J}||\nabla u|dx \geq \int_\Omega \frac{|\mathbf{J}|}{|\nabla v|}|\nabla u|^2 dx, \tag{24}$$

$$\frac{1}{2}\int_\Omega (|\mathbf{J}||\nabla v| - \frac{|\mathbf{J}|}{|\nabla v|}|\nabla u|^2) \leq \int_\Omega (|\mathbf{J}||\nabla v| - |\mathbf{J}||\nabla u|)dx \tag{25}$$

$$\leq \int_\Omega (|\mathbf{J}||\nabla v| - \frac{|\mathbf{J}|}{|\nabla v|}|\nabla u|^2)dx.$$

The equality in either (23) or (24) holds if and only if $u = v$.

This result gives rise to a simple iterative procedure. Let $(f, |\mathbf{J}|) \in H^{1/2}(\partial\Omega)\times L_2(\Omega)$ be an admissible pair. We start the iterative process with a harmonic function u_0 with the trace f on $\partial\Omega$. Let $u_{n-1} \in H^1(\Omega)$, such that

$$\frac{|\mathbf{J}|}{|\nabla u_{n-1}|} \in L^\infty_+(\Omega),$$

has been computed. Then we compute

$$\sigma_n = \frac{|\mathbf{J}|}{|\nabla u_{n-1}|}$$

and update the voltage potential as the unique solution to the Dirichlet problem

$$\nabla \cdot (\sigma_n \nabla u_n) = 0, \quad \text{in} \ \ \Omega,$$

$$u_n = f \quad \text{on} \ \ \partial\Omega.$$

Clearly, one need to ensure that each iteration satisfies $\frac{|\mathbf{J}|}{|\nabla u_{n-1}|} \in L^\infty_+(\Omega)$. In two dimensions, an almost two-to-one boundary voltage f is sufficient for this to hold, and further a posteriori sufficient conditions ensure convergence (see [57]). The computational effectiveness of this algorithm is demonstrated in Figures 4 and 6.

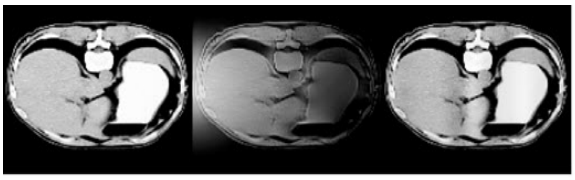

Figure 4: The conductivity images reconstructed by the simple iterative procedure: the original image (left), after 5 iterates (middle), after 50 iterates (right).

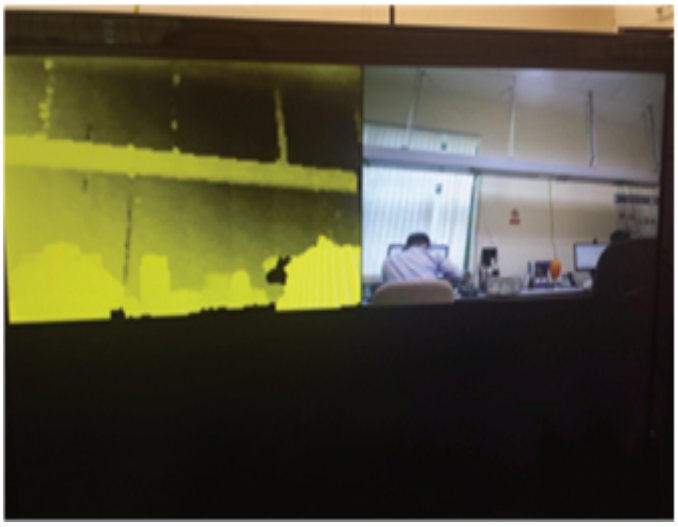

Figure 5: 3D image viewer running on BeagleBoard Xm.

4.3 An Alternating Split Bregman Algorithm

Let $(f, |\mathbf{J}|) \in H^{1/2}(\partial\Omega) \times L_2(\Omega)$. Consider the variational problem

$$\text{argmin}\{\int_\Omega |\mathbf{J}||\nabla v| dx : v \in H^1(\Omega), v = f \text{ on } \partial\Omega\}. \tag{26}$$

Suppose this problem has a solution in $H^1(\Omega)$. We construct some minimizing sequences as follows. Note that (26) belongs to a general class of problems

$$\text{argmin}\{G(u) + F(Lu) : u \in H^1(\Omega)\}, \tag{27}$$

where $L : H_1 \to H_2$ is a linear bounded operator, H_1, H_2 are real Hilbert spaces, and $G : H_1 \to R \cup \{\infty\}$ and $F : H_1 \to R \cup \{\infty\}$ are proper, convex and lower semi-continuous functions. Note that if for $H_1 = H_0^1(\Omega), H_2 = (L_2(\Omega))^n$, $Lu = \nabla u$ we fix

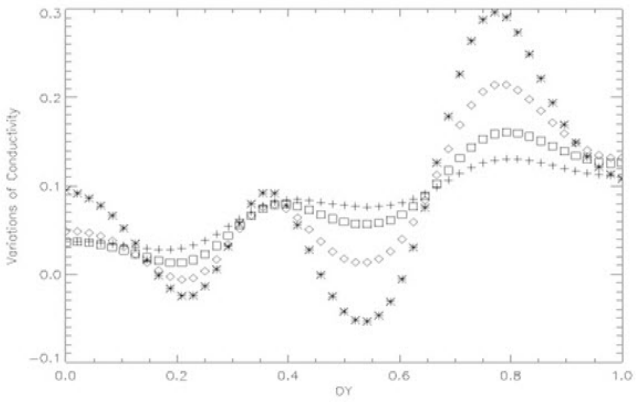

Figure 6: The slices of conductivity reconstructed by the simple iterative procedure: crosses - the initial approximation, squares - after 5 iterates, diamonds - after 50 iterates, stars - after 100 iterates. The latter almost coincides with the original conductivity.

$u_f \in H^1(\Omega)$ with $u_f = f$ on $\partial\Omega$ and define $F : (L_2(\Omega))^n \to R, G : H_0^1(\Omega))^n \to R$, such that

$$F(w) = \int_\Omega |\mathbf{J}||w + \nabla u_f| dx, \quad G(u) = 0,$$

then the problem (26) can be written in the form (27). Exploiting the Bregman's idea (see [19]) to link the method of multipliers and dual ascent method, in [29] the so-called alternating split Bregman algorithm was proposed to solve iteratively the problem (27) by reducing it to the unconstrained minimization problems at each iterate

$$u^{k+1} = \text{argmin}\{G(u) + \frac{1}{2}\|b^k + Lu^{k+1} - w\|_2^2 : u \in H_1\},$$

$$w^{k+1} = \text{argmin}\{F(u) + \frac{1}{2}\|b^k + Lu^{k+1} - w\|_2^2 : w \in H_2\},$$

$$b^{k+1} = b^k + Lu^{k+1} - w^{k+1}.$$

Unlike this approach, in [53] the dual problem for (27) was first formulated. This problem is well suited to a Douglas-Rachford splitting method which, in turn, lead naturally to the following alternating split Bregman algorithm for solving the problem (26).

Let $u_f \in H^1(\Omega)$ with $u_f = f$ on $\partial\Omega$.

Initialization. $b^0, d^0 \in (L_2(\Omega))^n$.

Step 1. For $k \geq 1$ solve

$$\nabla^2 u^{k+1} = \nabla \cdot (d^k(x) - b^k(x)) \text{ in } \Omega \; u^{k+1} = 0 \text{ on } \partial\Omega.$$

Step 2. Update

$$d^{k+1} = \Big\{ \max\{|\nabla u^{k+1} + \nabla u_f + b^k| - \frac{|\mathbf{J}|}{\lambda} \frac{\nabla u^{k+1} + \nabla u_f + b^k}{|\nabla u^{k+1} + \nabla u_f + b^k|} - \nabla u_f, if |\nabla u^{k+1} + \nabla u_f + b^k| \neq 0 \quad - \nabla u_f, if |\nabla u^{k+1} + \nabla

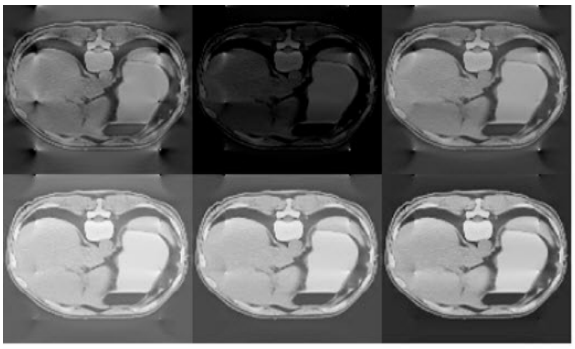

Figure 7: The conductivity images reconstructed from the interior data and non two-to-one boundary voltage with N = 1, 5, 10, 30, 50, 100 Bregman iterates.

Step 3. Update

$$b^{k+1} = b^k + \nabla u^{k+1} - d^{k+1}.$$

The convergence of this algorithm is established by the following

Theorem 12[MNT] *Let $\Omega \subset R^n, n \geq 2$ be a bounded region with the connected C^1, α boundary $\partial\Omega$. Assume that $|\mathbf{J}| > 0$ a.e. in Ω, where $\mathbf{J} \in (L_2(\Omega))^n$ is the current density generated by conductivity $\sigma \in C^\alpha(\Omega)$ by imposing the boundary voltage potential f. Then the voltage potential $\tilde{u}$ in Ω is the unique solution of the problem (26), and the sequences $b^k, d^k + \nabla u_f$, and $u^k + u_f$ generated by the alternating split Bregman algorithm converge weakly to $-\mathbf{J}/\lambda, \nabla\tilde{u}$, and $\tilde{u}$, respectively.*

In Figure 7 we demonstrate the computational effectiveness of this algorithm even for the non two-to-one boundary data.

4.4 On Constructing The Regularizing Algorithms

Applying Tikhonov's regularization for constructing minimizing sequences for a general class of functionals associated with the nonlinear PDEs was first proposed in [42] (see also [26]). In particular, regularizing the variational problem (26) also makes sense, because the corresponding functional is not strictly convex and non-differentiable. In [69] for the pair $(f, |\mathbf{J}|) \in H^{1/2}(\partial\Omega) \times L_2(\Omega)$ (not necessarily admissible) and for $\delta \geq 0, \varepsilon > 0$ the following variational problem was considered

$$\text{argmin}\{F_{\delta\varepsilon}[u] : u \in H^1(\Omega), u = f \text{ on } \partial\Omega\}, \tag{28}$$

where

$$F_{\delta\varepsilon}[u] = \int_\Omega |\mathbf{J}| \max\{|\nabla v|, \delta\} dx + \varepsilon \int_\Omega |\nabla u|^2 dx. \tag{29}$$

Theorem 13[TN] *Let $|\mathbf{J}| \in L_2(\Omega), |\mathbf{J}| \geq 0$, and the number $\varepsilon > 0$ be fixed. Then the functional (29) is weakly lower-semicontinuous in $H_0^1(\Omega$ and the variational problem (28) has a unique solution.*

Moreover, the following stability result takes place.

Theorem 14[TN] *Let* $(f, |\mathbf{J}|) \in H^{1/2}(\partial\Omega) \times L_2(\Omega)$ *be admissible and* $essinf(|\mathbf{J}|) \geq \alpha$ *for some* $\alpha > 0$. *Then there exists a number* $\delta > 0$, *such that (1)* $\forall\{|\mathbf{J}|_m \subset L_2(\Omega)\}, |\mathbf{J}|_m \to |\mathbf{J}|$ *in* $L_2(\Omega)$ *if one choose* $\varepsilon_m \to 0$, *so that*

$$\lim_{m\to\infty} \frac{\||\mathbf{J}| - |\mathbf{J}|_m\|^2}{\varepsilon_m} = 0,$$

and $\forall m$ *let* u_{ε_m} *be the solution of*

$$argmin\{F_{\delta\varepsilon_m}[u[: u \in H^1(\Omega), u = f \text{ on } \partial\Omega\}.$$

Then

$$\lim_{m\to\infty} infF_{\delta\varepsilon_m}[u_{\varepsilon_m}] = \lim_{m\to\infty} infF_{\delta 0}[u_{\varepsilon_m}] =$$

$$min\{F_{\delta 0}[u] : u \in H^1(\Omega), u = f \text{ on } \partial\Omega\} = min\{F_{00}[u] : u \in H^1(\Omega), u = f \text{ on } \partial\Omega\};$$

(2) $\exists\{u_{\varepsilon_k}\} : u_{\varepsilon_k} \to u^*$ *in* $L_q(\Omega), u^* \in L_q(\Omega) \cap BV(\Omega), 1 \leq q < n/(n-1), n/geq2$;
(3) if $u^* \in H_0^1(\Omega) \cap C(\overline{\Omega})$ *then* u^* *is the voltage potential corresponding to the pair* $(f, |\mathbf{J}|$.

Based on linearization of the power density operator (see [11]) in [12] the Dirichlet problem for the weighted 0-Laplace equation was numerically solved by the Levenberg-Marquardt iteration utilizing single and multiple "measurements" $W_i[\sigma] = \sigma|\nabla u_i|^2, (i = 1, 2, ..., m)$ in Ω, such that

$$\nabla \cdot (\sigma \nabla u_i) \text{ in } \Omega,$$

$$u_i = f_i \text{ on } \partial\Omega.$$

Assuming $\sigma \in H^l(\Omega), \sigma > 0, l > n/2$ and $f_i \in H^{l+1/2}(\partial\Omega)$, the power density operator was defined (see [11]) as a map $\mathcal{F}(\sigma) : H^l(\Omega) \to H^l(\Omega; R^m), \sigma \to (W_i)$, and its linearization - as the system

$$\nabla \cdot (\delta\sigma \nabla u_i) + \nabla \cdot (\sigma \nabla \delta u_i) = 0,$$

$$\delta\sigma|\nabla u_i|^2 + 2\sigma \nabla u_i \cdot \nabla u_i = \delta W_i.$$

Then the stability estimate [12] is given by

$$C_s^{-1}\|\delta\sigma - \delta\tilde{\sigma}\|_{H^s(\Omega)} \leq \|\delta\mathcal{F} - \delta\tilde{\mathcal{F}}\|_{H^s(\Omega;R^m)}$$

$$\leq C_s\|\delta\sigma - \delta\tilde{\sigma}\|_{H^s(\Omega)},$$

where $C_s = const > 0, s > n/2$.

Note that it follows from the theory of iterative methods for approximate solutions of inverse problems (see, e.g., [7]) that in order to update the conductivity at the kth iterate σ_k one can minimize the Tikhonov functional

$$T[\sigma] = \|W - \mathcal{F}(\sigma_k) - \mathcal{F}'(\sigma_k)(\sigma - \sigma_k)\|_{H_2}^2 + \alpha_k\|\sigma - \sigma_k\|_{H_1}^2,$$

where α_k are parameters of regularization, H_1, H^2 are Hilbert spaces, and $\mathcal{F}'$ is the Frechet derivative of $\mathcal{F}$. It results in the Levenberg-Marquardt algorithm

$$\sigma_{k+1} = \sigma_k + [\mathcal{F}'(\sigma_k)^*\mathcal{F}'(\sigma_k) + \alpha_k I]^{-1}\mathcal{F}'(\sigma_k)^*(W - \mathcal{F}(\sigma_k)),$$

where I is the identity operator. It should be mentioned that this algorithm produces only the α-sequences approximating the sought solution if α_k do not depend on *a priori* information about "measurements" W, particularly, about the level of noise. The analytical study of rates of convergence can be found in [7].

Acknowledgment

The authors are thankful to Adrian Nachman for his valuable suggestions.

References

[1] Allesandrini G, Critical points of solutions of elliptic equations in two variables, Ann. Scuola Norm. Sup. Pisa Cl. Sci. IV, 1987, 14 ,229–256.

[2] Alessandrini G, Stable determination of conductivity by boundary measurements, Appl. Anal., 1988, 27, 153-172.

[3] Alessandrini G, Global stability for a coupled physics inverse problems, Inverse Problems, 2014, 30, 075008 (10pp).

[4] Ammari H, E. Bonnetier E, Capdeboscq et al,, Electrical Impedance Tomography by Elastic Deformation, SIAM J. Appl. Math., 2008, 68, 1557 - 1573.

[5] Astala K and Päivärinta L, Calderón's inverse conductivity problem in the plane, Ann. of Math., 2006, 163, 265–299

[6] Arridge S R and Scherzer O, Foreword: Imaging from coupled physics, Inverse Problems, 2012, 28, 080201(2pp).

[7] Bakushinsky A B and Kokurin M Yu, Iterative Methods for Approximate Solution of Inverse Problems, Springer, The Netherlands, 2004.

[8] Bal G, Bonnetier E, Monard F and Triki F, Inverse diffusion from knowledge of power densities , Inverse Problems and Imaging, 2013, 7(2), 353–375.

[9] Bal G, Cauchy problem for Ultrasound Modulated EIT ,Anal. PDE, 2013, 6, no. 4, 751-775.

[10] Bal G, Hybrid problems and internal information, 2013, Inverse problems and applications: inside out. II, 325-368, Math. Sci. Res. Inst. Publ., 60, Cambridge Univ. Press, Cambridge, 2013.

[11] Bal G, Hybrid inverse problems and systems of partial differential equations, 2012, arXiv: 1210.0265.

[12] Bal G, Naetar W, Scherzer O, et al, The Levenberg-Marquardt iteration for numerical inversion of the power density operator, 2012, arXiv: 1211.6034.

[13] Bal G and Uhlmann G, Reconstruction of coefficients in scalar second-order elliptic equations from knowledge of their solutions, Comm. Pure Appl. Math., 2013, 66, 1629–1652.

[14] Bal G and Monard F, Inverse anisotropic diffusion from power density measurements in two dimensions , Inverse Problems, 2012, 29, 084001

[15] Bal G. and Monard F, Inverse anisotropic conductivity from power density measurements in dimensions $n \geq 3$, Comm. Partial Differential Equations, 2013, 38, 1183-1207.

[16] Bal G, Guo C, and Monard F, Inverse anisotropic conductivity from internal current densities, Inverse Problems, 2014, 30, 025001.

[17] Bayford R H, Bioimpedance Tomography (Electrical impedance tomography), Annu. Rev. Biomed. Eng., 2006, 8, 63–91.

[18] Borcea L, Electrical impedance tomography, Inverse Problems, 2002, 18, R99–136.

[19] Bregman L M, A relaxation method of finding a common point of convex sets and its application to the solution of problems of convex programming,1967, USSR Zh. Vycisl. Mat. i Mat. Fiz., 7, 620-631.

[20] Bukhgeim A L, Recovering a potential from Cauchy data in the two-dimensional case, J. Inverse Ill-Posed Probl, 2008, 16, 19–33.

[21] Calderon A P, On an inverse boundary value problem, Seminar on Numerical Analysis and Its Applications to Continuum Physics (Rio de Janeiro: Soc. Brasil. Mat.), 1980, 65–73.

[22] Capdeboscq Y, Fehrenbach J, de Gournay F et al., Imaging by modification: numerical reconstruction of local conductivities from corresponding power density measurements, SIAM J. Imag. Sci., 2009, 2 1003–1030.

[23] Cheney M, Isaacson D and Newell J C, Electrical impedance tomography, 1999, SIAM Rev., 41, 85–101.

[24] Crandall M G, Ishli H, and Lions P-L, User's guide to viscosity solutions of second order partial differential equations, Bull. AMS, 1992, 27, 1-67.

[25] Di Cristo M and Rondi L, Examples of exponential instability for inverse inclusion and scattering problems, Inverse Problems, 2003, 19, 685-701.

[26] Ekeland I and Temam R, Convex analysis and variational problems, North-Holland- Elsevier, 1976.

[27] Evans L, Partial Differential Equations. Graduate Studies in Mathematics, 19, AMS, NY, 1998.

[28] Gebauer B and Scherzer O, Impedance-acoustic tomography, SIAM J. Appl. Math., 2008, 69, 565-576.

[29] Goldstein T and Osher S, The split Bregman method for L1-regularized problems. SIAM Journal on Imaging Sciences, 2009, 2(2), 323-343.

[30] Hoell N, Moradifam A and Nachman A, Current density impedance imaging of an anisotropic conductivity in a known conformal class, SIAM J. Math. Anal., 2014, 46 , no. 3, 1820-1842.

[31] Isaacson D, Distinguishability of Conductivities by Electric Current Computed Tomography, IEEE Trans. on Medical Imaging, 1986, Vol. MI-5, No. 2, 91-95.

[32] Jerrard R L, Moradifam A and Nachman A, Existence and uniqueness of minimizers of general least gradient problems, 2013.

[33] Joy M L, Scott G C, and Henkelman R M, In vivo detection of applied electric currents by magnetic resonance imaging, Magn. Reson. Imaging, 1989, 7, 89-94.

[34] Joy M J, Nachman A, Hasanov K F et al, A new approach to Current Density Impedance Imaging (CDII), Proceedings ISMRM, No. 356, Kyoto, Japan, 2004.

[35] Kim S, Kwon O, Seo J K et al, On a nonlinear partial differential equation arising in magnetic resonance electrical impedance tomography, SIAM J. Math. Anal., 2002, 34, 511-526.

[36] Kim Y J, Kwon O, Seo J K et al., Uniqueness and convergence of conductivity image reconstruction in magnetic resonance electrical impedance tomography, Inverse Problems 2003, 19, 1213-1225.

[37] Kwon O, Lee J-Y, and Yoon J R, Equipotential line method for magnetic resonance electrical impedance tomography, Inverse Problems, 2002, 18, 108-1100.

[38] Kuchment P and Kunyansky L, Synthetic focusing in ultrasound modulated tomography, Inverse Probl. Imaging, 2010, 4, 665-673.

[39] Kuchment P and Kunyansky L, 2D and 3D reconstructions in acousto-electric tomography, Inverse Problems, 2011, 27, 055013.

[40] Kuchment P and Steinhauer D, Stabilizing inverse problems by internal data, Inverse Problems, 2012, 28, 084007 (20pp).

[41] Kwon O, Lee J Y, and Yoon J R, Equipotential line method for magnetic resonance electrical impedance tomography. Inverse Problems, 2002, 18, 1089-1100.

[42] Ladyzhenskaya O A and Uraltseva N N, Local estimates for greadients of solutions of non-uniformly elliptic and parabolic equations, Comm. Pure Appl. Math., 1970, 23, 677-703.

[43] Langer R E, An inverse problem in differential equations, Bull. Amer. Math. Soc., 1933, 39, 814–820.

[44] Lavandier B, Jossinet J and Cathignol D, Quantitative assessment of ultrasound-induced resistance change in saline solution Med. Biol. Eng. Comput., 2000, 38 150–155.

[45] Lavrent'ev M M, Romanov V G, and Shishatskii, Ill-Posed Problems of Mathematical Physics and Analysis, AMS, NY, 1986.

[46] Lee J Y, A reconstruction formula and uniqueness of conductivity in MREIT using two internal current distributions, Inverse Problems 2004, 20, 847–858.

[47] Lindqvist P, Notes on the p-Laplace equations, www.math.ntnu.no/ lqvist/p-laplace.pdf.

[48] Liu J, Seo J K, and Woo E J, A posteriori error estimate and convergence analysis for conductivity image reconstruction in MREIT, SIAM J. Appl. Math., 2012, 70, 2883-2903.

[49] Ma W, Nachman A, Elsaid N, et al., Anistropic impedance imaging using diffusion tensor and current density measurements, 2013.

[50] Mandache N, Exponential instability in an inverse problem for the Schrodinger equation, Inverse Problems, 2001, 17, 1435-1444.

[51] Montalto C and Stefanov P, Stability of coupled-physics inverse problems with one internal measurement, Inverse Problems, 2013, 29, 125004.

[52] Moradifam A, Nachman A, and Timonov A, A convergent algorithm for the hybrid problem of reconstructing conductivity from minimal interior data. Inverse Problems, 2012.

[53] Moradifam A, Nachman A and Tamasan A, Uniqueness of minimizers of weighted least gradient problems arising in conductivity imaging, 2013.

[54] Nachman A, Reconstructions from boundary measurements, Ann. Math., 1988, 128 531–576.

[55] Nachman A, Global uniqueness for a two-dimensional inverse boundary value problem, Ann. Math., 1996, 143, 71–96.

[56] Nachman A, Tamasan A, and Timonov A, Conductivity imaging with a single measurement of boundary and interior data, Inverse Problems, 2007, 23, 2551–2563.

[57] Nachman A, Tamasan A, and Timonov A, Recovering the conductivity from a single measurement of interior data, Inverse Problems, 2009, 25, 035014 (16pp).

[58] Nachman A, Tamasan A, and Timonov A, Reconstruction of planar conductivities in subdomains from incomplete data. SIAM J. Appl. Math., 2010, 70, 3342–3362.

[59] Nachman A, Tamasan A and Timonov A, Current density impedance imaging, Contemporary Mathematics, 2011, 559.

[60] Scott G C, Joy M L, Armstrong R L et al, Measurement of nonuniform current density by magnetic resonance, IEEE Trans. Med. Imaging, 1991, 10, 362-374.

[61] Scott G C, Joy M L, Armstrong R L et al, Sensitivity of magnetic-resonance current density imaging, J. Magn, Res., 1992, 97, 235–254.

[62] Song Y amd Seo J K, Conductivity and permittivity image reconstruction at the Larmor frequency using MRI, SIAM J. Appl. Math., 2013, 73, no. 6, 22622280.

[63] Sylvester J and Uhlmann G, 1987, A global uniqueness theorem for an inverse boundary value problem, Ann. Math., 125, 153–169.

[64] Seo J K, Yoon J R, Woo E J et al., Reconstruction of conductivity and current density images using only one component of magnetic field measurements, IEEE Trans. Biomed. Eng., 2003, 50, 1121-1124.

[65] Seo J K, Jeon K, Lee C O et al., Non-iterative harmonic B_z algorithm in MREIT, Inverse Problems, 2011, 27, 085003.

[66] Seo J K and Woo E J, Magnetic resonance electrical impedance tomography, SIAM Rev., 2011, 53, 40-68.

[67] Seo J K, Kim D-H K, Lee J et al., Electrical tissue property imaging using MRI at dc and Larmor frequency, Inverse Problems, 2012, 28, 084002 (26pp).

[68] Sternberg P and Ziemer W P, generalized motion by curvature with a Dirichlet condition, J. Diff. Eq., 1994, 114, 580-600.

[69] Tamasan A and Nashed Z, Structural stability in a minimization problem and applications to conductivity imaging, Inverse Problems and Imaging, 2011, 1(5), 219-236.

[70] Tamasan A, Veras J, Conductivity imaging by the method of characteristics in the 1-Laplacian. Inverse Problems, 2012;28:084006, 13pp.

[71] Tamasan A, Timonov A, and Veras J, Stable reconstruction of regular 1-Harmonic maps with a given trace at the boundary. Applicable Analysis, 2014, DOI: 10.1080/00036811.2014.918260.

[72] Tikhonov A N, On uniqueness of the solution of the problem of electric prospecting. Doklady Akad. Nauk SSSR, 69(6), 797800 (in Russian).

[73] Widlak T and Scherzer O, Hybrid tomography for conductivity imaging, Inverse Problems, 2012, 28, 084008(28pp).

[74] Zhang H and Wang L, Acousto-electric tomography, Proc. SPIE, 2004, 5320 145–149.

Alexandru Tamasan
Department of Mathematics
University of Central Florida
4392 Andromeda Loop N
Orlando, FL 32816
Email: alexandru.tamasan@ucf.edu
Alex Timonov
Division of Mathematics and Computer Science
University of South Carolina Upstate
800 University Way
Spartanburg, SC 29303
Email: atimonov@uscupstate.edu

Received 14.10.2014, Accepted 26.10.2014.